

# A combination of concave/convex surfaces for field-enhancement optimization: the indented nanocone

Aitzol García-Etxarri,<sup>1,2,\*</sup> Peter Apell,<sup>2,3</sup> Mikael Käll<sup>3</sup> and Javier Aizpurua<sup>2</sup>

<sup>1</sup>Department of Materials Science and Engineering, Stanford University, Stanford, California 94305, United States

<sup>2</sup>Materials Physics Center CSIC-UPV/EHU and Donostia International Physics Center DIPC, Paseo Manuel de Lardizabal 5, Donostia-San Sebastian 20018, Spain

<sup>3</sup>Department of Applied Physics, Chalmers University of Technology, SE-412 96 Göteborg, Sweden

\*[aitzol@stanford.edu](mailto:aitzol@stanford.edu)

**Abstract:** We introduce a design strategy to maximize the Near Field (NF) enhancement near plasmonic antennas. We start by identifying and studying the basic electromagnetic effects that contribute to the electric near field enhancement. Next, we show how the concatenation of a convex and a concave surface allows merging all the effects on a single, continuous nanoantenna. As an example of this NF maximization strategy, we engineer a nanostructure, the indented nanocone. This structure, combines all the studied NF maximization effects with a synergistic boost provided by a Fano-like interference effect activated by the presence of the concave surface. As a result, the antenna exhibits a NF amplitude enhancement of  $\sim 800$ , which transforms into  $\sim 1600$  when coupled to a perfect metallic surface. This strong enhancement makes the proposed structure a robust candidate to be used in field enhancement based technologies. Further elaborations of the concept may produce even larger and more effective enhancements.

© 2012 Optical Society of America

**OCIS codes:** (250.5403) Plasmonics; (240.6680) Surface plasmons; (300.6340) Spectroscopy, infrared; (240.6695) Surface-enhanced Raman scattering.

---

## References and links

1. L. Novotny, and N. Van Hulst, "Antennas for light," *Nature Photon.* **5**, 83-90 (2011).
2. H. Xu, E. Bjerneld, M. Käll, and L. Börjesson, "Spectroscopy of Single hemoglobin molecules by surface enhanced raman scattering," *Phys. Rev. Lett.* **83**, 4357-4360 (1999).
3. F. Neubrech, A. Pucci, T. Cornelius, S. Karim, A. Garcia-Etxarri, and J. Aizpurua, "Resonant plasmonic and vibrational coupling in a tailored nanoantenna for infrared detection," *Phys. Rev. Lett.* **101**, 2-5 (2008).
4. T. Rindzevicius, Y. Alavverdyan, A. Dahlin, F. Höök, D. S. Sutherland, and M. Käll, "Plasmonic sensing characteristics of single nanometric holes," *Nano Lett.* **5**, 2335 (2005).
5. A. Dmitriev, C. Hägglund, S. Chen, H. Fredriksson, T. Pakizeh, M. Käll, and D. S. Sutherland, "Enhanced nanoplasmonic optical sensors with reduced substrate effect," *Nano Lett.* **8**, 3893 (2008).
6. H. A. Atwater, and A. Polman, "Plasmonics for improved photovoltaic devices," *Nature Mat.* **9**, 205-213 (2010).
7. A. C. Atre, A. García-Etxarri, H. Alaeian, and J. A. Dionne, "Toward high-efficiency solar upconversion with plasmonic nanostructures," *J. Opt.* **14**, 024008 (2012).
8. Z. Liu, W. Hou, P. Pavaskar, M. Aykol, and S. B. Cronin, "Plasmon resonant enhancement of carbon monoxide catalysis," *Nano Lett.* **11**, 1111-1116 (2011).

9. H. Xu, J. Aizpurua, M. Käll, and P. Apell, "Electromagnetic contributions to single-molecule sensitivity in surface-enhanced Raman scattering," *Phys. Rev. E* **62**, 4318-4324 (2000).
10. P. Nordlander and C. Oubre, "Plasmon hybridization in nanoparticle dimers," *Nano Lett.* **4**, 899-903 (2004).
11. K. Li, M. Stockman, and D. Bergman, "Self-similar chain of metal nanospheres as an efficient nanolens," *Phys. Rev. Lett.* **91**, 227402 (2003).
12. M. Stockman, "Nanofocusing of optical energy in tapered plasmonic waveguides," *Phys. Rev. Lett.* **93**, 137404 (2004).
13. S. Vedantam, H. Lee, J. Tang, J. Conway, M. Staffaroni and E. Yablonovitch, "A Plasmonic dimple lens for nanoscale focusing of light," *Nano Lett.* **9**, 34473452, (2009).
14. D. K. Gramotnev and S. I. Bozhevolnyi, "Plasmonics beyond the diffraction limit," *Nature Photon.* **4**, 83-91 (2010).
15. F. J. García De Abajo, and A. Howie, "Retarded field calculation of electron energy loss in inhomogeneous dielectrics," *Phys. Rev. B* **65**, 115418 (2002).
16. F. J. García de Abajo, and A. Howie, "Relativistic electron energy loss and electron-induced photon emission in inhomogeneous dielectrics," *Phys. Rev. Lett.* **80**, 5180-5183 (1998).
17. C. F. Bohren and D. R. Huffman, "*Absorption and Scattering of Light by Small Particles*" (Wiley, New York, 1983).
18. E. J. Zeman and G. C. Schatz, "An accurate electromagnetic theory study of surface enhancement factors for Ag, Au, Cu, Li, Na, Al, Ga, In, Zn, and Cd," *J. Phys. Chem.* **91**, 634-643 (1987).
19. Y. Korniyushin, "Plasma oscillations in porous samples," *Sci. Sinter.* **36**, 43-50 (2004).
20. H. Xu, E. J. Bjerneld, J. Aizpurua, P. Apell, L. Gunnarsson, S. Petronis, B. Kasemo, C. Larsson, F. Hook, and M. Käll, "Interparticle coupling effects in surface-enhanced Raman scattering," *Proc. SPIE* **4258**, 35-42 (2001).
21. I. Romero, J. Aizpurua, G. W. Bryant, and F. J. García De Abajo, "Plasmons in nearly touching metallic nanoparticles: singular response in the limit of touching dimers," *Opt. Express* **14**, 9988-99 (2006).
22. E. Prodan, C. Radloff, N. J. Halas, and P. Nordlander, "A hybridization model for the plasmon response of complex nanostructures," *Science* **302**, 419 (2003).
23. J. Aizpurua, F. J. García de Abajo, and G. W. Bryant, "Mapping the plasmon resonances of metallic nanoantennas," *Nano Lett.* **8**, 631 (2008).
24. A. Weber-Bargioni, A. Schwartzberg, M. Cornaglia, A. Ismach, J. J. Urban, Y. Pang, R. Gordon, J. Bokor, M. B. Salmeron, D. F. Ogletree, P. Ashby, S. Cabrini, and P. J. Schuck, "Hyperspectral nanoscale imaging on dielectric substrates with coaxial optical antenna scan probes," *Nano Lett.* **11**, 1201 (2011).
25. T. J. Seok, A. Jamshidi, M. Kim, S. Dhuey, A. Lakhani, H. Choo, P. J. Schuck, S. Cabrini, A. M. Schwartzberg, J. Bokor, E. Yablonovitch, and M. C. Wu, "Radiation engineering of optical antennas for maximum field enhancement," *Nano Lett.* **11**, 2606 (2011).
26. C. Forestiere, A. J. Pasquale, A. Capretti, G. Miano, A. Tamburrino, S. Y. Lee, B. M. Reinhard, and L. Dal Negro, "Genetically engineered plasmonic nanoarrays," *Nano Lett.* **12**, 2037-2044 (2012).
27. T. Feichtner, O. Selig, M. Kiunke, and B. Hecht, "Evolutionary optimization of optical antennas," *Phys. Rev. Lett.* **109**, 127701 (2012).
28. D. P. Fromm, A. Sundaramurthy, P. J. Schuck, G. Kino, and W. Moerner, "Gap-dependent optical coupling of single "bowtie" nanoantennas resonant in the visible," *Nano Lett.* **4**, 957-961 (2004).
29. P. B. Johnson and R. W. Christy, "Optical constants of the noble metals," *Phys. Rev. B* **6**, 43704379 (1972).
30. J. Aizpurua, S. P. Apell, and R. Berndt, "Role of the tip shape in light emission from the scanning tunneling microscope," *Phys. Rev. B* **62**, 2065-2073 (2000).
31. F. J. García de Abajo and J. Aizpurua, "Numerical simulation of electron energy loss near inhomogeneous dielectrics," *Phys. Rev. B* **56**, 15873-15884 (1997).
32. J. Aizpurua, A. Howie, and F. J. García de Abajo, "Valence-electron energy loss near edges, truncated slabs, and junctions," *Phys. Rev. B* **60**, 11149-11162 (1999).
33. S. P. Apell, P. M. Echenique, and R. H. Ritchie, "Sum rules for surface plasmon frequencies," *Ultramicroscopy* **65**, 53-60 (1996).
34. E. Moreno, S. G. Rodrigo, S. I. Bozhevolnyi, L. Martín-Moreno, and F. J. García-Vidal, "Guiding and focusing of electromagnetic fields with wedge plasmon polaritons," *Phys. Rev. Lett.* **100**, 023901 (2008).
35. B. Lukyanchuk, N. I. Zheludev, S. A. Maier, N. J. Halas, P. Nordlander, H. Giessen, and C. Tow Chong, "The Fano resonance in plasmonic nanostructures and metamaterials," *Nature Mater.* **9**, 707-715 (2010).
36. A. Cvitkovic, N. Ocelic, and R. Hillenbrand, "Analytical model for quantitative prediction of material contrasts in scattering-type near-field optical microscopy," *Optics Expr.* **15**, 8550-8565 (2007).
37. S. Sheikholeslami, A. García-Etxarri, and J. A. Dionne, "Controlling the interplay of electric and magnetic modes via Fano-like plasmon resonances," *Nano Lett.* **11**, 39273934 (2011).
38. F. Neubrech, A. García-Etxarri, D. Weber, J. Bochterle, H. Shen, M. Lamy De La Chapelle, G. W. Bryant, J. Aizpurua, and A. Pucci, "Defect-induced activation of symmetry forbidden infrared resonances in individual metallic nanorods," *Appl. Phys. Lett.* **96**, 213111 (2010).

## 1. Introduction

The rational design of effective optical antennas [1] is challenging and necessary to push the limits of several emerging technologies such as field-enhanced spectroscopies [2,3], plasmonic biosensing [4,5], and plasmon enhanced photovoltaics and photocatalysis [6–8]. Various structures, such as dimers [9, 10] and plasmonic lenses [11] have been proposed and adopted to obtain electromagnetic hot-spots with very large field enhancements of up to 1000 times the incident electromagnetic field amplitude. These huge enhancements are obtained mainly through electromagnetic coupling of metallic nanoparticles. The field-enhancements produced by isolated nanostructures are less spectacular, typically not higher than 100 in amplitude. In this contribution, we first introduce the elementary strategies for maximizing the near-field enhancement around metallic structures and secondly, we combine these building blocks on a single continuous nanostructure, the indented nanocone, to show the potential of combining all the enhancing effects in one single continuous nanostructure.

The electromagnetic field enhancement in the proximity of metallic nanostructures is an intrinsic property of surface plasmons excited at certain resonant frequencies. This enhancement is a consequence of the localization of the fields in the vicinities of the metal-dielectric interface. In structures supporting propagating Surface Plasmon Polaritons (SPP-s), the localization of fields can be optimized by means of different tapering strategies [12–14]. On small structures instead, the optical response is dominated by Localized Surface Plasmon Resonances (LSPR-s) and localization of the fields is determined by the geometrical details of the structures and by the coupling to other systems. The strong dependence of the optical response on the characteristics of the geometry and the coupling make the optimization of the field enhancement a challenging task in nanophotonics. In the next section we summarize the most relevant effects that lead to an increase of the field-enhancement in a plasmonic nanoantenna whose optical response is dominated by LSPR-s. Some of the effects cannot be isolated and very often different effects are expressed jointly. However, it is useful to identify them separately for conceptual clarity.

## 2. Ingredients of the field enhancement

To gain insights about the nature of the different near field enhancing effects, we first introduce a simple non-retarded analytical model and later verify the identified effects with numerical simulations obtained by using the Boundary Element Method (BEM) [15, 16] to solve Maxwell's equations.

Let us assume the generic polarizability tensor components  $\alpha_{jj}$  of an ellipsoidal particle ( $P$ ) of volume  $V$  in a medium ( $M$ ) [17]

$$\alpha_{jj}(\omega) = \frac{4\pi\epsilon_0 V}{L_j} \frac{\epsilon_P(\omega) - \epsilon_M(\omega)}{\epsilon_P(\omega) - \epsilon_M(\omega) + \epsilon_M(\omega)/L_j} = \alpha_0 f(\omega), \quad (1)$$

where  $\epsilon_P/\epsilon_M/\epsilon_0$  are the dielectric functions of the particle/medium/vacuum respectively, and  $L_j$  is the so called depolarization factor, corresponding to the direction of the component  $j$  of the applied field, that only depends on the shape of the particle.  $\alpha_0 = 4\pi\epsilon_0 V/L_j$  is the static polarizability of the particle.

For illustration purposes we will use a Drude dielectric function to describe the optical response of the metal particle in this non-retarded analytical model.

$$\epsilon_P/\epsilon_0 = 1 - \frac{\omega_p^2}{\omega(\omega + i\gamma)} \quad (2)$$

being  $\omega_p$  the bulk plasma frequency of the metal and  $\gamma$  the Drude damping. We will consider the surrounding medium to be vacuum. The maximum field enhancement is proportional to the

absolute value of  $\alpha$ . Linearizing Eq. 1 around its resonant energy, the field enhancement can be expressed as

$$|E/E_0| \propto \frac{V}{L_j V_d} \frac{\sqrt{L_j}/2}{[(\sqrt{L_j} - \Omega)^2 + (\Gamma/2)^2]^{1/2}}, \quad (3)$$

where  $\Omega = \omega/\omega_p$  and  $\Gamma = \gamma/\omega_p$ .  $V_d$  accounts for an apparent volume corresponding to the evaluation point. Separating the static polarizability prefactor from the resonant part with resonance frequency  $\omega_p \sqrt{L_j}$ , it is easy to notice that the enhancement depends on both the shape of the object through  $L_j$  as well as the characteristic length scale of the object related to  $V$ , and the material properties ( $\omega_p$  and  $\gamma$ ) as we will now describe in more detail.

*Material:* Taking Eq. 3 as a reference, it is easy to conclude that the resonant value of the field enhancement is correlated with the Drude damping of the material ( $\gamma$ ). Smaller  $\gamma$  factors give rise to sharper resonances and thus, to higher values of the maximum field enhancement in the surroundings of the spheroid.

Fig. 1(a) illustrates this dependence. We calculate the field enhancement spectra of three 5 nm spheres 1 nm away from their surface for 3 different materials with different Drude damping factors. We choose Copper, Gold and Silver as an example. The Drude damping factors of these materials are  $\gamma_{Cu} = 0.0955$  eV,  $\gamma_{Au} = 0.07088$  eV and  $\gamma_{Ag} = 0.02125$  eV [18]. The maximum value of the near field increases as the Drude damping factor of the material decreases. Note that the resonant wavelength is also modified due to the different bulk plasma frequencies ( $\omega_p$ ) of the materials. Based on this argument and in the spirit of trying to maximize the near field response of a nanostructure, we will choose silver as the material to use for the rest of the study.

*Size effect:* The near field enhancement achieved through the excitation of localized surface plasmons decays with the cube of the distance from the surface of the object. In Eq. 3 this decay is accounted by the apparent volume  $V_d$ . The maximum field enhancement will occur right at the surface of the object where  $V \equiv V_d$ . When fixing the distance between the surface of the object and evaluation point, higher volumes will give rise to field enhancement values closer to the maximum achievable values, since  $V/V_d$  will asymptotically approach unity as the volume of the object is increased. In general, we can conclude that, structures with larger volumes, will allow higher field enhancements in their vicinities.

Fig. 1(b), analyzes this effect. We calculate the near-field spectra in the proximity of silver spheres of different volumes 1 nm outside their surface. For spherical particles,  $V = (4/3)\pi a^3$  and  $V_d = (4/3)\pi(a+b)^3$ , where  $a$  is the radius of the sphere and  $b$  the separation between the surface of the sphere and the observation point. Finally,  $V/V_d = (a/(a+b))^3$ . Keeping  $b$  unmodified, the maximum field enhancement will increase as  $a$  becomes larger. It will ultimately saturate, since  $V/V_d$  will tend to unity for large values of  $a$ .

*Lightning rod effect:* The field enhancement obtained by increasing the volume of the structure can still be enhanced through further localization of the near-field response with the use of sharper geometries. The reason behind this relies on the lightning rod effect. Large variations of the surface curvature produce a large potential gradient in very reduced areas. Therefore, large field values are produced at sharp structures.

The static polarizability  $\alpha_0 = \frac{4\pi\epsilon_0 V}{L_j}$  contains the lightning rod effect in terms of the depolarization factor  $L_j$  in the denominator. As the shape of the object gets sharper, which for the prolate spheroid happens when the major axis  $a$  is much larger than the minor axis  $b = c$ , the static polarizability increases accordingly. As the spheroid becomes more elongated along the  $j$  direction,  $L_j$  approaches zero. For a prolate ellipsoid the depolarization factor for the major axis  $L_a$  can be expressed as [19]

$$L_a = \frac{b^2 c^2}{a^2 b^2 + a^2 c^2 + b^2 c^2}. \quad (4)$$

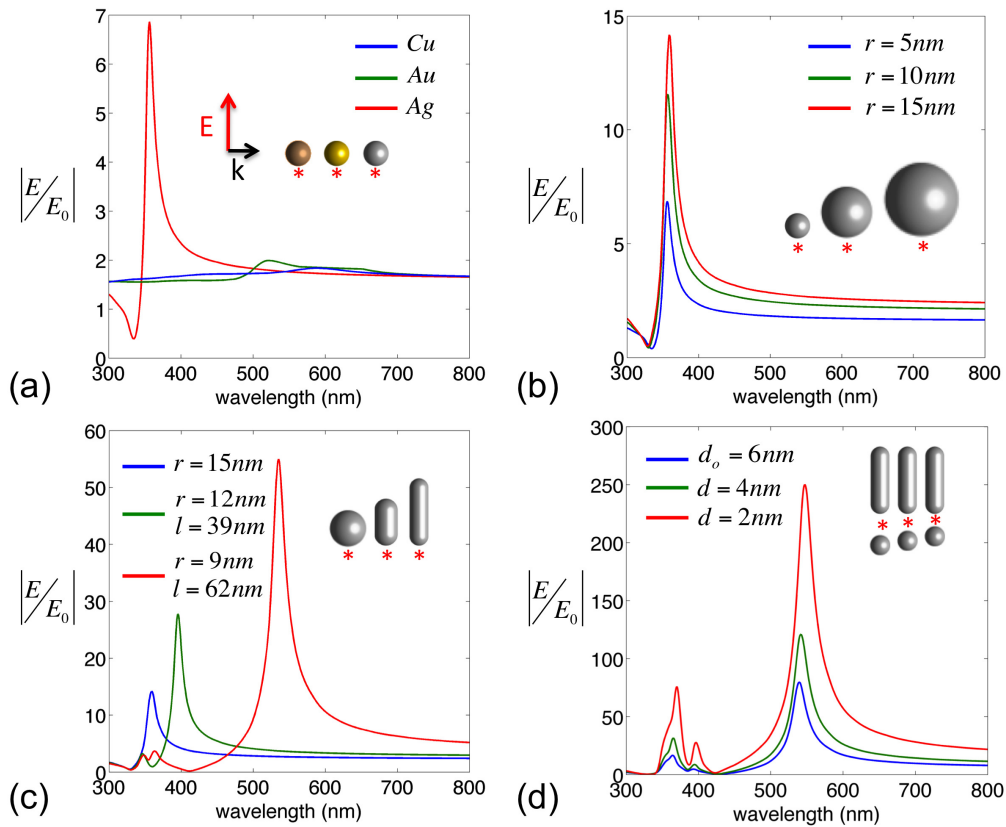


Fig. 1. Evolution of the near-field amplitude enhancement spectra 1 nm above the surface of one of the extremities of different metallic structures when changing different parameters of the system. Calculations were performed by using the BEM. Incident electric field polarization is chosen to be parallel to the rod axis. Vacuum is assumed as the embedding material. a) *Material*: Near field enhancement in the surroundings of three different 5 nm radius spheres made of Copper, Gold and Silver. Smaller damping factors give rise to sharper resonances and higher values for the maximum field enhancement. b) *Size effect*: Modification of the volume of the system  $V$ , keeping the distance between the surface and the observation point constant. The field enhancement on the surroundings of three silver spheres of different radii ( $r = 5, 10, 15\text{ nm}$ ) is calculated. The near field enhancement increases with the volume, saturating for large volumes as  $V$  approaches the apparent volume  $V_d$ . c) *Lightning rod effect*: Modification of the length keeping the volume and the distance to the observation point of the system constant, so that  $V/V_d \approx 1$ , for different rod radii  $r$ . Sharper structures give rise to higher values of the field enhancement due to the lightning rod effect. d) *Coupling*: System composed of a rod and a sphere, for different separation distances ( $d$ ) between the rod and the sphere. The near field in this latter case is evaluated at the center of the gap. Smaller separation distances produce a stronger coupling and a higher field enhancement.

When written in this form, it is helpful to connect the depolarization factor with a well-defined measure of the sharpness of a surface, i.e. its curvature. For a surface with principal radii of curvature  $\rho_1$  and  $\rho_2$  at a point, we can define the mean curvature as  $H = \frac{1}{2}(\frac{1}{\rho_1} + \frac{1}{\rho_2})$  and the Gaussian, or total, curvature as  $K = \frac{1}{\rho_1\rho_2}$ . We can now express the depolarization  $L_a$  (Eq. 4) in terms of the Gaussian curvature  $K_{a,b,c}$  at the endpoints of the ellipsoid in the direction of the coordinate axes

$$L_a = \frac{a^2/K_a}{a^2/K_a + b^2/K_b + c^2/K_c} \approx \frac{1}{2b^2K_a} \quad (5)$$

since for an elongated ellipsoid ( $b = c$ )  $K_a = (\frac{a}{b^2})^2 \gg K_{b,c}$ . Consequently, we can express the enhancement from the lightning rod effect as being directly proportional to the Gaussian curvature.

We illustrate this effect in Fig. 1(c), by calculating the near field spectra of three structures with different sharpness. To avoid the interplay of any apparent size effects, we elongate a sphere and transform it into a thinner rod while maintaining the total volume and the distance to the observation point constant. In this way, we ensure that the  $V/V_d \approx 1$ . We can observe in the near-field spectra of Fig. 1(c) how the enhancement increases as the radius of the structure decreases and therefore the Gaussian curvature increases. A complementary way of exploiting this effect on an antenna is to use of sharp antenna terminations instead of rounded endings.

*Coupling:* Coupling of the electromagnetic response of a nanostructure to adjacent metallic systems is known to produce field localization and correspondingly enhancement of the near-field at the region in-between the structures [2, 9, 20–22]. We illustrate this effect in Fig. 1(d) by calculating the near field spectra of a coupled system composed by a 62 nm long silver rod with 9 nm radius silver sphere. We calculate the near-field at the center of the gap between the rod and the sphere for different separation distances  $d$  ( $d = 6$  nm, 4 nm and 2 nm). An increase of the near-field maximum can be observed as the separation distance becomes smaller. This effect is connected with the appearance of a coupled bonding plasmon that belongs to the whole system arising from the symmetric coupling of the dipolar plasmons of each nanostructure.

Due to the in-phase excitation of the rod and the sphere, considering them as equipotential surfaces, the potential drop due to the external field is concentrated at the gap. The field enhancement increases proportionally with the inverse of the separation distance [20]. Fig. 1(d) corroborates this assumption. Taking the peak near-field enhancement for the largest separation distance as a reference ( $NF_o = 80$  for  $d_o = 6$  nm), the NF for the other gap sizes should scale as

$$NF_{max}(d) = \frac{NF_o}{d/d_o} \quad (6)$$

According to Eq. 6, for  $d = 4$  nm and  $d = 2$  nm, the corresponding peak field enhancements should take values of 120 and 240 respectively. These values are in excellent agreement with the maximum field enhancement values calculated by solving Maxwell's equations numerically using the BEM (121 and 250).

Typically, by means of coupling, the field enhancement can be increased about an order of magnitude with respect to that of the isolated systems. Interestingly, in this particular example of a rod coupled to a small sphere, the spectral response of the coupled system does not red shift when the particles are approached as could be expected. Being the sphere much smaller than the rod, the rod dominates the spectral behavior of the system making the expected red shift due to the coupling between the structures negligible. This particular detail could be specially valuable for spectroscopic applications such as SERS and SEIRA. Carefully designing the rod one could engineer its resonances to match the absorption frequencies of the molecules under study [23]

and in a second step gain an extra order of magnitude of field enhancement by coupling it to a small sphere without modifying the resonance frequency of the coupled system.

Some optimization strategies based on a combination of some or all of these effects have been applied recently to obtain large field enhancements. We can cite among others [24–27] the case of bowtie antennas [28], where a combination of interparticle coupling and sharp ends produce large enhancements in the plasmonic antenna gap, or the case of the plasmonic lens [11] where three particles of different size are brought together combining effects of size, coupling and sharpness of the structures to produce huge field enhancements. All these studies suggest the use of discrete structures to obtain the enhancing effect. In this contribution, we propose the use of a continuous structure based on a metallic cone where we will induce size, coupling and lightning rod effects with the help of concave and convex deformations of the surfaces at the metallic apex of a cone. We call this structure the indented nanocone.

### 3. Indented nanocone

We introduce in this section a novel nanostructure that merges simultaneously all the concepts described above. We will consider that the structure is made of silver, using dielectric data from the literature to characterize its optical response [29].

A big metallic cone, when polarized along its main axis, provides a large volume that will ensure maximum field enhancement values in the vicinities of the structure. Complementarily, the sharp the cone apex allows to localize very efficiently the induced surface charge density [30]. Figure 2(a) shows the optical extinction cross section of a 300 nm height silver cone of aperture angle of  $30^\circ$  and radius of curvature at the apex of 10 nm. Incident polarization is indicated at the inset of Fig. 2(a). Figure 2(b) shows the corresponding NF spectrum calculated 1 nm below the cone apex. We observe that the highest NF enhancement for such a structure occurs at  $\lambda = 985$  nm. The surface charge density associated with this localized plasmon mode and the near-field map at the cone apex are shown in Fig. 2(c) and Fig. 2(d) respectively. Field enhancements of around 40 times the field amplitude of the incoming electric field can be obtained in the proximity of this finite conical structure.

The optical properties of metallic concave and convex geometries offer the possibility to control the symmetry of the surface charge density of the lowest order plasmonic modes [31, 32]. Figure. 3(a) and Fig. 3(b) show the surface charge density profile for the lowest energy mode of a convex and a concave perfect metallic surface respectively. A concave surface (Fig. 3(a)) presents a symmetric profile for the surface charge density, piling up charge at the edge. On the complementary convex surface, instead, sum-rules ensure that the lowest energy mode will present an anti-symmetric surface charge density profile [31, 33]. As a consequence, a node of the charge is produced at the convex area [34], as shown in Fig. 3(b). The combination of a concave and a convex surface thus produces inevitably a change of the sign of the surface charge density at one type of surface with respect to the other. It is possible to create in this way areas where the surface charge density is forced to change sign within the same continuous structure. Consequently, a combination of concave and convex surfaces permits to exploit in the same closed geometry both the aspect of localization, caused by the presence of the sharp edges, as well as the aspect of coupling, happening between facing surfaces with induced surface charge density distributions of opposite sign.

A combination of concave and convex surfaces in the same continuous structure can be realized in an indented nanocone structure as the one depicted in Fig. 4(a). Illuminated by light polarized along the cone axis, this geometry allows for a combination of the different near field maximization factors introduced above: a large volume, localization of the charge density at the edges and coupling of plasmonic modes in close proximity.

We show in Fig. 5(a) the optical extinction cross section of a silver indented nanocone. The

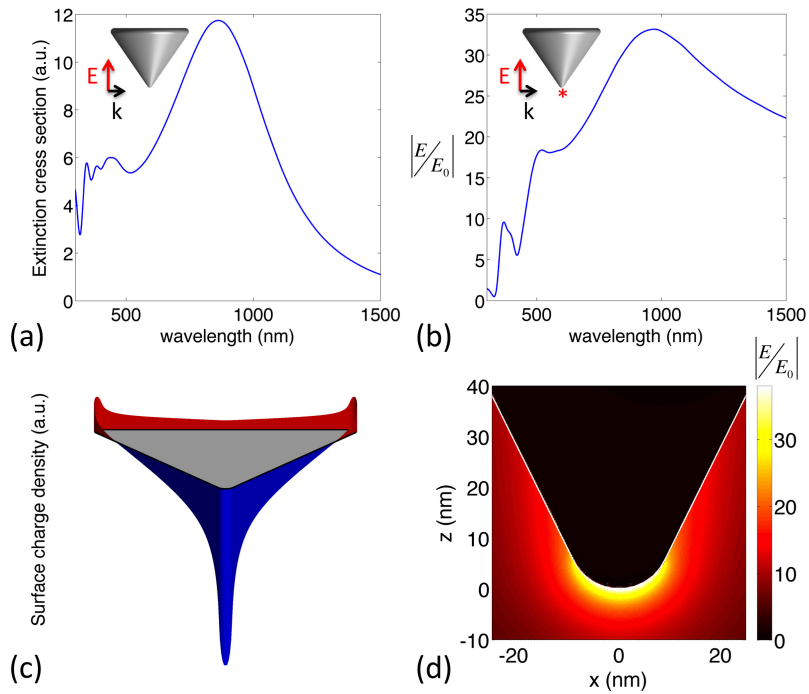


Fig. 2. Optical response of a 300 nm height, 10 nm radius and  $30^\circ$  aperture angle silver nanocone a) Extinction cross section in arbitrary units with incident light as displayed in the inset. b) Near-field amplitude enhancement spectra of the silver cone calculated 1 nm below the cone apex. c) Surface charge density profile of a cross section of the cone for  $\lambda = 985$  nm. Blue and red areas indicate regions where the surface charge density is negative and positive respectively. The charge density distribution presents azimuthal symmetry. d) Near-field enhancement distribution of the cone for normal incident light of  $\lambda = 985$  nm polarized along the cone axis. The optical response of the cone is mainly characterized by a strong localization at the cone apex giving rise to a maximum field enhancement of  $\sim 40$ .

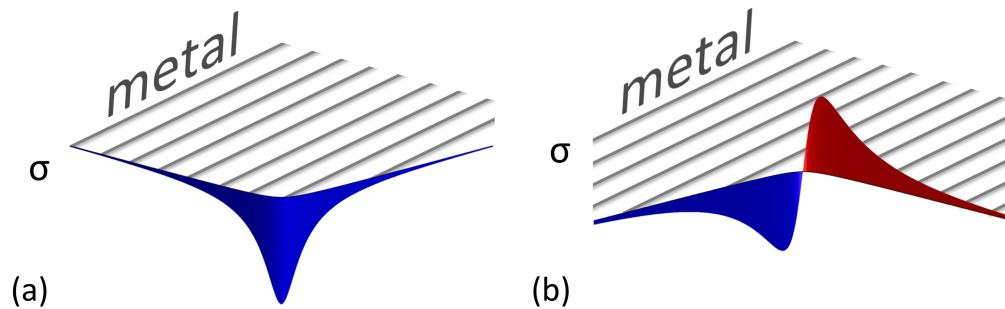


Fig. 3. Surface charge density ( $\sigma$ ) plots, in arbitrary units, for the lowest energy modes of a a) convex and b) concave perfect metallic surface. The lowest energy mode for the convex surface presents a symmetric charge density distribution. On a concave structure instead, the surface charge density mode is antisymmetric, presenting a node at the concavity. For an elaborate discussion about these simulations see Ref. [31]. A combination of both kinds of surfaces allows to localize the surface charge density in sharp regions as well as to couple the charges with opposite sign excited at both sides of the concave surface.

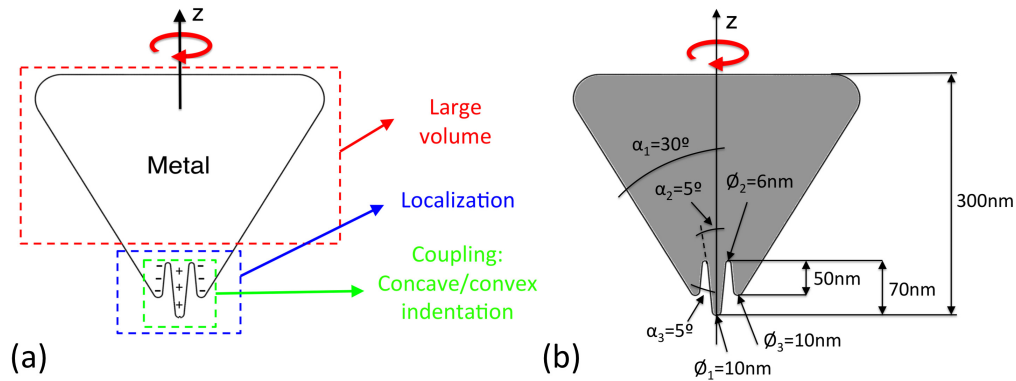


Fig. 4. Cross section of the geometry of the indented nanocone. a) The combination of the four field enhancement ingredients (a large volume, the localization of the charge density at the edges and the coupling), permits the creation of a field enhancement of  $\sim 800$  at the tip apex (see Fig. 5) b) Geometrical details of the proposed structure. The upper arrow indicates the rotational symmetry axis of the geometry.

far-field spectrum of the indented nanocone shows strong similarities with that corresponding to the smooth cone presented in the inset of Fig. 5(a). However, a new mode emerging at the near infrared (IR) range of the spectrum appears as a predominant feature. This new mode is very intense and narrow and it seems natural to assign its emergence to the presence of the geometrical features of the indented nanocone. To confirm the nature of this new intense peak, we calculate the surface charge density at the lowest resonant energy ( $\lambda = 1061$  nm) as shown in Fig. 5(c). As expected, the surface charge density is piled up on the convex zones of the geometry (indented nanoconical arms and central tip). Therefore, the local fields show maximum value and localization in these areas. In the concave area, a zero in the surface charge density is induced, forcing the charge density to change sign and effectively acting as a source of coupling and polarization of the system as explained above.

Interestingly, the new spectral feature presents the typical lineshape of a Fano-like interference effect [35]. As previously mentioned, the concave surface imposes a change of sign of the surface charge density, somewhat decoupling the response of the central tip from the response of the overall object. As a consequence of this forced variation of the sign of the charge, the rest of the smaller convex central tip becomes uniformly charged and its response mimics the response of an electric monopole [36]. If we were to isolate the central tip from the overall object, this monopolar resonance would be unexcitable (dark). It is, in fact, the concave geometry that allows for the excitation of this mode by imposing a zero in the surface charge density at the convex area. In this sense, the combination of a convex and concave surface presents a new strategy, complementary to symmetry breaking [35, 37, 38], for the activation of dark modes in nanoscale optical systems. The prominent Fano-like resonance arises from the spectral interference of this previously dark monopolar mode of the central tip and the broader bright mode of the entire cone.

The resulting near-field map for the resonant wavelength ( $\lambda = 1061$  nm) is shown in Fig. 5(d). A maximum field-enhancement of  $\sim 800$  in amplitude is achieved for realistic parameters of the arm length and their respective curvatures (see Fig. 4(b) for geometrical details).

The reason for this huge enhancement does not rely on the sharp curvature of the central tip of the indented nanocone, as one intuitively could think on a first approach. Calculations of the field enhancement for the small central tip of the indented nanocone (same curvature) only

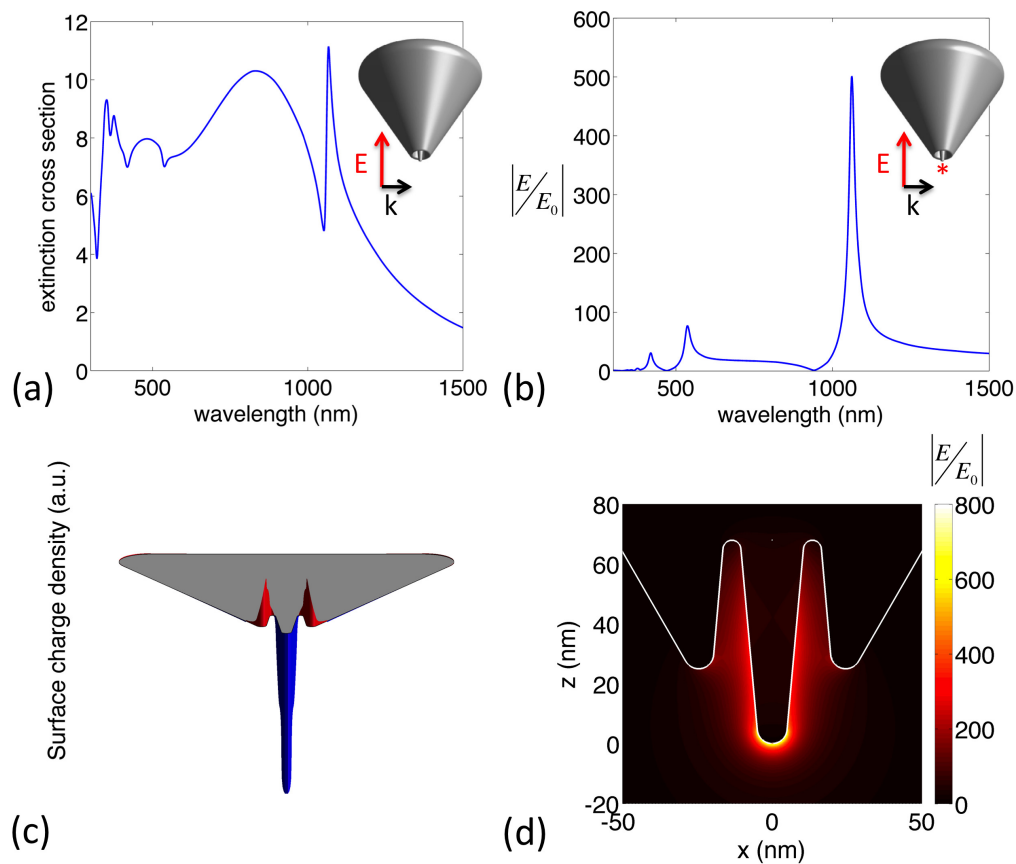


Fig. 5. Optical response of the indented nanocone depicted in Fig. 4. a) Extinction cross section in arbitrary units for the incident polarization displayed in the inset. b) Near-field enhancement spectra of the silver indented nanocone calculated 1 nm below the cone apex. c) Cross section of the surface charge density profile of the indented nanocone for  $\lambda = 1061$  nm (in arbitrary units) d) Near-field enhancement distribution of the system for normal incident light at  $\lambda = 1061$  nm polarized along the cone axis. The proposed structure, allows for the combination of the field enhancement ingredients introduced in Fig. 1, giving rise to field enhancement factors of  $\sim 800$  in amplitude.

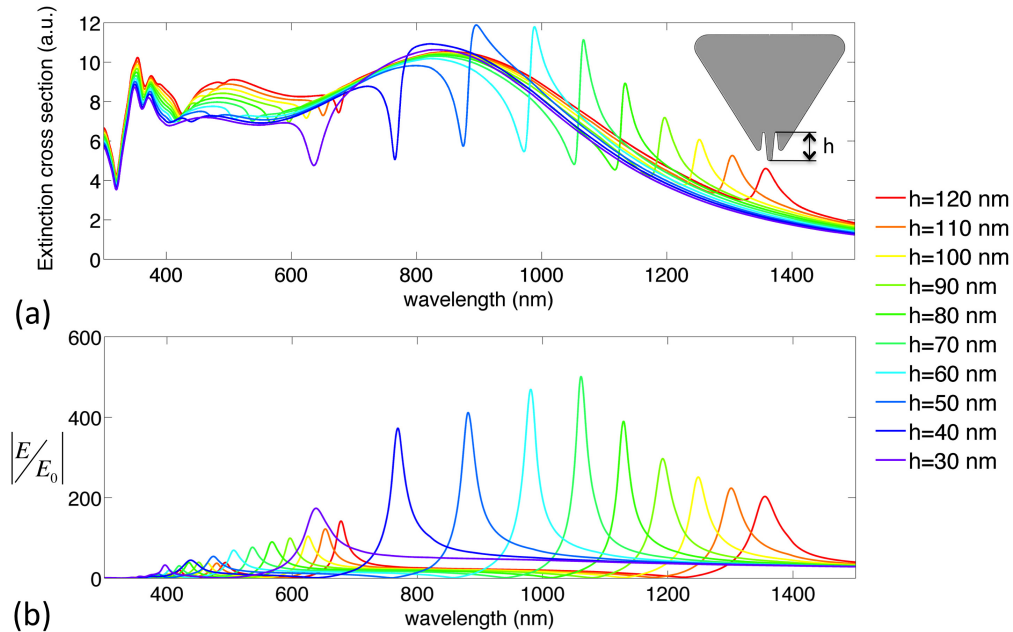


Fig. 6. Optical response of the silver indented nanocone for different central tip lengths  $h$ . a) Extinction cross section in arbitrary units. The lineshape of the Fano-like interference can be tailored by modifying the central tip length. b) Near-field enhancement spectra calculated 1 nm below the cone apex. The maximum field enhancement occurs for  $h = 70$  nm.

reach enhancements of the order of one order of magnitude in amplitude. It is the combination of all the ingredients mentioned in this work that makes this structure a unique continuous structure providing such enhancement. In that sense, the role of the convex part of the indented nanocone is crucial for two different reasons. First, it allows for a geometrical localization of the surface charge density, and second, it activates the interference between the dipolar and the monopolar modes. This gives rise to a spectral region where the surface charge densities of the two resonances interfere constructively boosting the near field response of the system. In conclusion, the concave surface allows for a synergistic combination of all the ingredients for the field enhancement through the activation of a Fano-like interference effect involving a localized mode at the tip apex and a broader mode extended to the whole structure.

Modifying the depth of the small central tip allows for a tailoring of this interference effect. Fig. 6(a) plots the extinction cross section of the indented nanocone for different central tip lengths ( $h$ ). The lineshape of the Fano-like interference changes from a dip to a peak depending on the relative spectral position of the dark monopolar mode of the central tip with respect to the resonant frequency of the bright dipolar mode of the cone. Fig. 6(b) presents the near field enhancement spectra 1 nm below the cone apex. The peak near field enhancement is maximized when the near fields produced by the central tip and the cone interfere constructively in an optimum manner. This occurs for a central tip length of 70 nm, which corresponds to the chosen length for the calculations presented in the previous figures.

It is possible to go further in the enhancing strategy by providing an additional external coupling to this structure. To this end, we locate an indented nanocone facing a perfect metallic surface acting as a mirror for different separation distances. The image charges on the perfect metal mimic the presence of an additional indented nanocone facing the original structure on

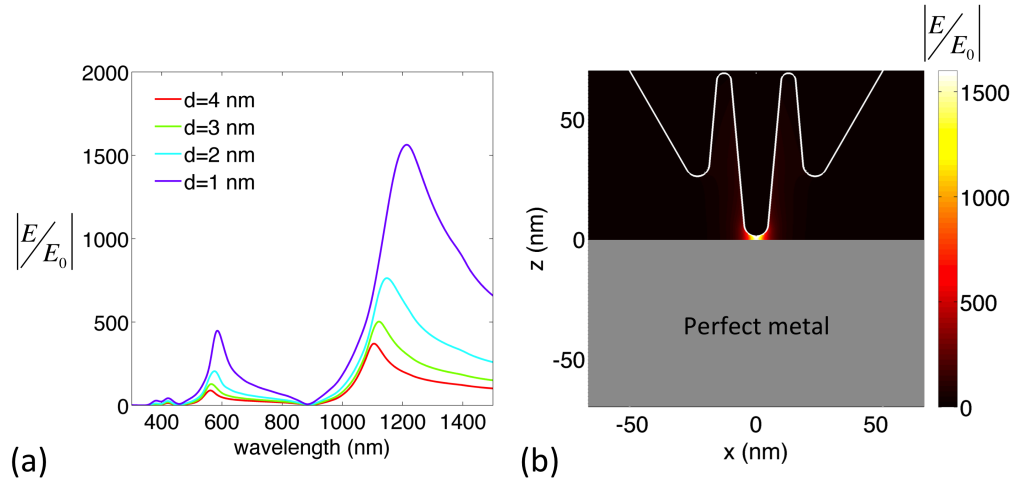


Fig. 7. Indented nanocone coupled to a perfect metallic surface. a) Near-field amplitude spectra for different separation distances  $d = (4, 3, 2, 1 \text{ nm})$ . b) Near field map for a separation distance of 1 nm at  $\lambda = 1212 \text{ nm}$ . The extra coupling results in a maximum field enhancement of  $\sim 1600$  in amplitude.

a bowtie configuration. Fig. 7(a) shows the NF spectra 0.5 nm below the nanocone tip for 4 different separation distances ( $d = 4, 3, 2, 1 \text{ nm}$ ). The extra coupling results in a field enhancement of  $\sim 1600$  for a separation distance of 1 nm. The near field distribution of the coupled system on resonance ( $\lambda = 1212 \text{ nm}$ ) is shown in Fig. 7(b) for a separation distance of 1 nm, showing a very strong concentration of the fields at the gap between the indented nanocone and the metallic surface.

#### 4. Conclusion

In summary, we have identified the key electromagnetic effects that can be used to optimize the near-field enhancement of a metallic nanostructure and applied them to design a continuous nanoantenna where the field enhancement reaches about the largest values reported in the literature. Further modifications of this concept may lead to even larger factors. To obtain these enhancing factors appropriate values for the dielectric response and damping of the metals have been used as well as realistic parameters for the cone lengths, curvatures and indentations. This structure, or different variations of the same concepts, could be very beneficial in photonic applications based on field enhancement such as surface enhanced spectroscopy and light harvesting for photovoltaics.

#### Acknowledgments

A.G.E. thanks Ashwin C. Atre for assistance preparing Fig.6 and Fig.7. This work was supported by the Eortek-2011 project nanoiker of the Department of Industry of the Basque Government, project FIS2010-19609-C02-01 of the Spanish Ministry of Science and Innovation and the Swedish Foundation for Strategic Research through the project RMA08 Functional Electromagnetic Metamaterials.